# Molecular dynamics of C-peptide of ribonuclease A studied by replica-exchange Monte Carlo method and diffusion theory

Giovanni La Penna $^{a,*}$ , Ayori Mitsutake $^{b,\dagger}$ , Masato Masuya $^{c,\ddagger}$ , Yuko Okamoto $^{d,e,\S}$ 30th October 2018

- <sup>a</sup> National Research Council, Institute for Macromolecular Studies, Section of Genova, Via De Marini 6, 16149 Genova, Italy
- <sup>b</sup> Department of Physics, Faculty of Science and Technology, Keio University, Yokohama, Kanagawa 223-8522, Japan
- $^{c}$  Computing and Communications Center, Kagoshima University, Kagoshima 890-0065, Japan
- <sup>d</sup> Department of Theoretical Studies, Institute for Molecular Science, Okazaki, Aichi 444-8585, Japan
- <sup>e</sup> Department of Functional Molecular Science, The Graduate University for Advanced Studies, Okazaki, Aichi 444-8585, Japan

#### Abstract

Generalized-ensemble algorithm and diffusion theory have been combined in order to compute the dynamical properties monitored by nuclear magnetic resonance experiments from efficient and reliable evaluation of statistical averages. Replica-exchange Monte Carlo simulations have been performed with a C-peptide analogue of ribonuclease A, and Smoluchowski diffusion equations have been applied. A fairly good agreement between the calculated and measured <sup>1</sup>H-NOESY NMR cross peaks has been obtained. The combination of these advanced and continuously improving statistical tools allows the calculation of a wide variety of dynamical properties routinely obtained by experiments.

- \* e-mail: lapenna@ge.ismac.cnr.it
- † e-mail: ayori@rk.phys.keio.ac.jp
- <sup>‡</sup> e-mail: masatom@cc.kagoshima-u.ac.jp
- § e-mail: okamotoy@ims.ac.jp

# 1 Introduction

In the study of protein folding, a crucial step is the understanding of secondary structure formations. The construction of  $\alpha$ -helices and  $\beta$ -sheets from disordered structures and their interconversion is mainly driven by hydrophobic effects combined with dispersive interactions and intramolecular hydrogen-bond formations [1, 2]. Salt bridges and strong electrostatic interactions can either compete with this driving force or assist the secondary structure formation, by introducing long-range average distance constraints. The latter can be influenced by the characteristics of the solvent and/or ions eventually enclosed in pre-folded configurations.

In order to address these complications related to the sequence variability in real proteins' secondary structures, many experiments are performed on relatively short peptide fragments that *in vitro* adopt conformations similar to those revealed in the entire proteins. These fragments, therefore, may be considered as independent modules [3] of the original protein [4]. These experiments allow a great simplification, replacing most of the protein matrix with the solvent, while keeping in the molecule the relevant interactions. On the other hand, short peptides visit many conformations, and thus the usage of statistical tools and computer simulations is required for the interpretation of experimental data.

Computer simulations in canonical ensemble based on Boltzmann weight factor, however, tend to get trapped in states of energy local minima, and it is very difficult to obtain accurate statistical averages even for small peptide systems. Generalized-ensemble algorithms are based on artificial, non-Boltzmann weight factors and perform random walks in potential energy space, which efficiently alleviates the multiple-minima problem (for a recent review, see Ref. [5]). After a single production run, one can calculate accurate canonical-ensemble averages for a wide range of temperatures [5]. Because of the very construction of the generalized-ensemble algorithms, however, the information of molecular dynamics is lost, and only static average values can be obtained by these methods.

Nuclear magnetic resonance (NMR) has become an attractive technique because it allows one to monitor both structural statistics (average distances) and molecular dynamics (stochastic rotation of vectors) at an atomistic level and in different solvent/temperature conditions. These features are, however, intimately linked together in the experimental data, particularly in those data routinely measured to obtain structures, *i.e.*, the <sup>1</sup>H-NOESY cross peaks (CPs).

In order to calculate dynamical properties from NMR experiments, a diffusive model has been designed and casted in a Smoluchowski diffusion equation. This equation has been solved by matrix expansion methods and by using a mode-coupling approximation [6, 7]. This procedure allows the description of the time-correlation functions (TCFs) that govern NMR experiments through the computation of a suitable set of configurational averages.

In this Letter we propose to combine the above two powerful computational approaches: generalized-ensemble algorithm and diffusion theory, which allows rigorous calculations of molecular dynamics inferred by NMR experiments.

A C-peptide analogue of ribonuclease A is here considered. The C-peptide of ribonuclease A is one of the smallest peptides that is known to form  $\alpha$ -helix conformations and has been extensively studied by circular dichroism (CD) [8] and NMR [9, 10] spectroscopies. The peptide has also been studied by computer simulations [11]–[14]. Nevertheless, a

quantification of the conformational population and of its effect on the experimental data was not possible and the standard methods used to analize NMR relaxation data cannot be applied [15]. We employed one of the commonly used generalized-ensemble algorithms, replica-exchange Monte Carlo (REMC) [16], to calculate statistical averages and various dynamical quantities were successfully obtained by the diffusion theory.

In section 2 the two mehotds are summarized and computational details are given. In section 3 the results of the statistics and the NMR CPs are discussed in a unique frame. In section 4 conclusions and perspectives are presented.

# 2 Methods

# 2.1 Replica-exchange method

We first briefly review the replica-exchange method (REM) [16] (see, for instance, Refs. [17, 5] for details).

The system for REM consists of M non-interacting copies (or, replicas) of the original system in the canonical ensemble at M different temperatures  $T_m$  ( $m=1,\dots,M$ ). We arrange the replicas so that there is always exactly one replica at each temperature. Then there is a one-to-one correspondence between replicas and temperatures. Let  $X = \{\dots, x_m^{[i]}, \dots\}$  stand for a "state" in this generalized ensemble. Here,  $x_m^{[i]}$  stands for the state of the i-th replica (at temperature  $T_m$ ); the superscript i and the subscript m in  $x_m^{[i]}$  label the replica and the temperature, respectively. Each state  $x_m^{[i]}$  is specified by the coordinates  $q^{[i]}$  (and momenta  $p^{[i]}$ ) of all the atoms in replica i.

A simulation of REM is then realized by alternately performing the following two steps. Step 1: Each replica in canonical ensemble of the fixed temperature is simulated simultaneously and independently for a certain MC or MD steps. Step 2: A pair of replicas, say i and j, which are at neighboring temperatures  $T_m$  and  $T_n$ , respectively, are exchanged:  $X = \left\{ \cdots, x_m^{[i]}, \cdots, x_n^{[j]}, \cdots \right\} \longrightarrow X' = \left\{ \cdots, x_m^{[j]}, \cdots, x_n^{[i]}, \cdots \right\}$ . The transition probability of this replica exchange is given by the Metropolis criterion:

$$w(X \to X') \equiv w\left(x_m^{[i]} \mid x_n^{[j]}\right) = \min\left(1, \exp\left(-\Delta\right)\right) , \tag{1}$$

where

$$\Delta = (\beta_m - \beta_n) \left( E\left(q^{[j]}\right) - E\left(q^{[i]}\right) \right) . \tag{2}$$

Here,  $E\left(q^{[i]}\right)$  and  $E\left(q^{[j]}\right)$  are the potential energy of the *i*-th replica and the *j*-th replica, respectively. In the present work we employ Monte Carlo algorithm for Step 1. When the potential energy depends on temperature as in the present case (see Eq. (13) below), we should use the following  $\Delta$  instead of that in Eq. (2) [18] (see also [19]):

$$\Delta = \beta_m \left( E\left(q^{[j]}; T_m\right) - E\left(q^{[i]}; T_m\right) \right) - \beta_n \left( E\left(q^{[j]}; T_n\right) - E\left(q^{[i]}; T_n\right) \right) . \tag{3}$$

A random walk in "temperature space" is realized for each replica, which in turn induces a random walk in potential energy space. This alleviates the problem of getting trapped in states of energy local minima.

The canonical expectation value of a physical quantity A at temperature  $T_m$  ( $m = 1, \dots, M$ ) can be calculated by the usual arithmetic mean as follows:

$$\langle A \rangle_{T_m} = \frac{1}{N_{sim}} \sum_{t=1}^{N_{sim}} A\left(x_m^{[i]}(t)\right) ,$$
 (4)

where  $N_{sim}$  is the total number of measurements made at temperature  $T_m$ . Note that the above summation is taken over different replicas i ( $i = 1, \dots, M$ ) that happens to correspond to the fixed temperature  $T_m$  at the moment of measurement. The expectation values at any intermediate temperature can, in principle, be calculated by the multiple-histogram reweighting techniques [17], but in this article we limit our discussions to the above M temperature values.

## 2.2 Calculation of NMR parameters

In this subsection we briefly review recent advances of diffusion theory [6, 7] that are applied to the calculation of the <sup>1</sup>H-NOESY NMR cross peak intensities (CPs).

The CP intensities  $O_{h,k}$  at mixing time  $t_m$  between spin h and spin k can be calculated by the following equation:

$$O_{h,k}(t_m) = \frac{R_{h,k}}{\Delta} \exp(-\sigma t_m) \sinh(\Delta t_m) , \qquad (5)$$

where  $R_{h,k}$ ,  $\Delta$ , and  $\sigma$  are all functions of the following spectral densities (see Refs. [6, 7] for details):

$$J_{h,k}(\omega) = 2 \int_{0}^{\infty} \cos(\omega t) \, TCF_{h,k}(t) \, dt \, . \tag{6}$$

Here,  $TCF_{h,k}$  is a time-correlation function of 2nd-rank tensor components of the vectors  $\mathbf{r}_{h,k}$  joining proton h and proton k. These TCFs at temperature T have the form [20]

$$TCF(t) = \sum_{M=-2}^{2} \left\langle \left[ D_{M,0}^{(2)*}(\Omega(t)) / r(t)^{3} \right] \left[ D_{M,0}^{(2)}(\Omega(0)) / r(0)^{3} \right] \right\rangle_{T}, \tag{7}$$

where  $D_{M,0}^{(2)}$  are irreducible spherical tensors [21], and  $\Omega$  and r are the direction and the modulus, respectively, of the given H-H vector involved in the NOESY CP (subscripts h and k are henceforth suppressed for clarity).

In order to separate the effect of the modulus from the orientation of the unit vector (direction) in the above TCF, we also calculate the orientational TCF from

$$TCF_O(t) = \sum_{M=-2}^{2} \left\langle \left[ D_{M,0}^{(2)*}(\Omega(t)) \right] \left[ D_{M,0}^{(2)}(\Omega(0)) \right] \right\rangle_T = P_2(\cos[\theta(t)]) , \qquad (8)$$

where  $P_2$  is the 2nd-order Legendre polynomial. The orientational mobility can be described by the correlation time  $\tau$  that is the integral of  $TCF_O$ :

$$\tau = \int_{0}^{\infty} TCF_O(t) dt.$$
 (9)

The mode-coupling diffusion (MCD) theory of the dynamics of a biological macromolecule in solution is adopted for the computation of the above TCFs of Eqs. (7) and (8). The MCD approach [22, 23] can be briefly summarized as follows. Given a polymer of  $N_a$  beads of friction coefficients  $\zeta_i$  and coordinates  $\mathbf{r}_i$ , connected by  $N_b$  bonds  $(\mathbf{l}_i, i = 1, ..., N_b)$ , the dynamics of each variable  $\mathbf{l}_i$ , is regulated by the operator L, adjoint to the diffusion Smoluchowski operator D:

$$\frac{\partial \mathbf{l}}{\partial t} = L\mathbf{l}; \quad L = \sum_{i,j=1}^{N_a} \left[ \nabla_i \mathbf{D}_{i,j} \nabla_j - (\nabla_i U/k_B T) \mathbf{D}_{i,j} \nabla_j \right], \tag{10}$$

where U is the potential energy of the beads as a function of the bead coordinates,  $k_B$  is the Boltzmann constant, T is the absolute temperature, and  $\mathbf{l}$  is the  $3 \times N_b$  dimensional array containing all the bond vectors  $\mathbf{l}_i$ .

By expanding the conditional probability (solution to the Smoluchowski equation) in a complete set of eigenfunctions of L, the time autocorrelation function (TCF) of any coordinate-dependent dynamic variable with zero average f(t) may be expressed in the standard form

$$\langle f(t) f(0) \rangle_T = \sum_i \langle f \psi_i \rangle_T \langle \psi_i f \rangle_T \exp(-\lambda_i t) ,$$
 (11)

where  $-\lambda_i$  and  $\psi_i$  are respectively the eigenvalues and the normalized eigenfunctions of the operator L:

$$L\psi_i = -\lambda_i \psi_i \ . \tag{12}$$

This eigenvalue equation becomes a matrix equation, with the matrix elements being equilibrium averages at temperature T (see Refs. [6, 7] for details). In the present work, we use the replica-exchange Monte Carlo method for the calculation of these averages (see Eq. (4)).

## 2.3 Computational details

The configurational statistics of a C-peptide analogue [9] with the amino-acid sequence AETAAAKFLRAHA and uncharged N- and C- termini have been simulated by replica-exchange Monte Carlo method. Residue His 12 was protonated in order to better match the NMR experimental conditions of pH 5.2. Other charged residues were Glu 2<sup>-</sup>, Lys 7<sup>+</sup>, and Arg 10<sup>+</sup>. The number of atoms in the model was 195.

The total "potential energy" function E(q;T) that we used is the sum of the conformational energy term of the solute  $E_P(q)$  and the solvation free energy term  $E_{SOL}(q;T)$  for the interaction of the peptide with the surrounding solvent:

$$E(q;T) = E_P(q) + E_{SOL}(q;T) . (13)$$

The parameters in the conformational energy as well as the molecular geometry were taken form ECEPP/2 [24]. The sigmoidal, distance-dependent dielectric function of Ref. [25] was used.

The solvation free energy that we used is given by a linear combination of the solvent-accessible surface area (SASA)  $A_i$  of each non-hydrogen atom i:

$$E_{SOL}(T_0) = \sum_{i} \sigma_i A_i , \qquad (14)$$

where  $\sigma_i$  are the proportionality constants,  $T_0 = 298$  K, and the dependence on the coordinates q is now suppressed. The temperature dependence of the solvation free energy was taken into account, following the prescription in Ref. [26]:

$$E_{SOL}(T) = \frac{T}{T_0} E_{SOL}(T_0) + H_{SOL}(T_0) \left(1 - \frac{T}{T_0}\right) - C_{SOL}(T_0) \left[T \ln\left(\frac{T}{T_0}\right) + T_0 - T\right] , \quad (15)$$

where  $H_{SOL}$  and  $C_{SOL}$  are enthalpy and heat capacity, respectively [26].

The SASA was calculated by the computer code NSOL [27]. The computer code KONF90 [11] was used, and MC simulations based on REM were performed. In each Monte Carlo sweep all the independent dihedral angles except for the peptide-bond dihedral angles  $\omega$ , which were fixed at 180 degrees, were updated once and the Metropolis test was performed for each update. The number of changeable torsion angles was then 55 and the maximum torsional change was  $\pm 180$  degrees.

For REMC we used 10 replicas. The corresponding temperatures were 200, 233, 276, 317, 370, 432, 504, 588, 686, and 800 K. These temperatures were chosen to span the temperature range between 200 and 800 K and to contain the temperature of the NMR experiments (276.15 K). The initial conformations were randomly generated. The replica exchange was tried every 20 MC sweeps. For an optimal performance of REMC simulations, the acceptance ratios of replica exchange should be sufficiently uniform and large (say, > 10%). The acceptance ratio was indeed found to be in the range 14–24%, and we observed that each replica underwent an unbiased random walk in the potential energy space (and that each temperature underwent a random walk in the replica space). After 1,100,000 MC sweeps of equilibration, the REMC production run of 3,000,000 MC sweeps for each replica was made. The configurations were stored every 10 MC sweeps for data analyses. This amounts to 300,000 configurations for each temperature (or each replica).

As for the diffusion equation, the first step is to approximate atoms or group of atoms in the molecule as friction points. In the present model, friction points were located on 55 heavy atoms (beads) among the total of 195 atoms. The friction was computed by using Stokes' law with stick boundary conditions with Stokes' radii obtained summing the accessible surface area to a spherical probe of 0 radius (ASA0) of the atoms grouped in the bead [28]. The Stokes' radii ranged from 0.09 nm ( $C_{\alpha}$  in all residues that include  $H_{\alpha}$  only) to 0.24 nm (the last portion of Arg 10 side chain, that includes  $N_{\epsilon}$ ,  $C_{\zeta}$ ,  $N_{\eta 1}$ ,  $N_{\eta 2}$  and all the bonded hydrogen atoms). The water viscosity  $\eta$  was 0.001 Pa s and it was assumed independent of temperature.

The second step is to assess the convergence of the used basis set in solving the eigenvalue equation for the adjoint of the diffusion operator. Both the long-time sorting procedure (LTSP) [29] and the maximum correlation approximation (RM2-II basis set of MCA) [7] were applied to select the most important terms of the infinite mode-coupling basis set. The results coupling the five 1st-order lowest-rate modes for 1st-rank variables up to the 2nd-order for 2nd-rank variables (MCA with e=5 in the notations of Ref. [7]) were almost identical with the 2nd-order LTSP using up to 600 basis functions (data not shown). Therefore, the MCA basis set built with e=5 (240 basis functions) was used for all of the following calculations.

No significant changes in the ten lowest-rate 1st-order/1st-rank relaxation modes were observed reducing the number of configurations from 300,000 down to 10,000. Therefore, for the calculations of the statistical averages required to solve the diffusion equation and to compute the TCFs at each temperature, 10,000 of the 300,000 recorded configurations were used.

# 3 Results and Discussion

The C-peptide is relatively rich in hydrophobic residues (Ala, Leu, and Phe) and, therefore, in a water environment is expected to be mainly in  $\alpha$ -helix conformation. On the other hand, the presence of charged residues, namely, Glu 2<sup>-</sup> (near the N-terminus), Lys 7<sup>+</sup>, Arg 10<sup>+</sup>, and His 12<sup>+</sup> (near the C-terminus), will have significant effects on the conformational states of the peptide. In Fig. 1 the average  $\alpha$ -helicity as a function of residue number (or, probability of each residue being in the  $\alpha$ -helix state) is shown for four different temperatures (276 K, 370 K, 504 K, and 686 K). Here, we considered that a residue is in the  $\alpha$ -helix state when the backbone dihedral angles  $(\phi, \psi)$  fall in the range  $(-70 \pm 30^{\circ}, -37 \pm 30^{\circ})$ , and Eq. (4) was used to calculate the average helicity. At the lowest temperature (T = 276 K) among the four, residues 4-12 are in helical state (especially, residues 6-11 are completely helical), which is exactly the same location of  $\alpha$ -helix as found in the corresponding structure from the X-ray experiments of the entire ribonuclease A [30]. Helicity decreases as the temperature is raised because of the increased thermal fluctuations. High helicity persists up to T = 504 K (especially in residues 6-11), and finally at the highest temperature among the four (T = 686 K), extended helical conformation ceases to exist. Note also that the N-terminus is not helical even at 276 K in agreement with the NMR experiments [9].

Fig. 2 shows the behaviour of the average total helicity (or, average total number of helical residues) as a function of temperature. As was observed in Fig. 1, the residues near the N-terminus are rarely in helical state, and this is the reason why even at the lowest temperature (T = 200 K) the average total number of helical residues is only about 8. The slight decrease of helicity between 370 K and 500 K is due to residues 6, 7, and 12 that lose  $\alpha$ -helical population, while the further decrease beyond 500 K involves the demolition of the remaining  $\alpha$ -helix in residues 8-11. The disorder in configurational statistics beyond 600 K still keeps part of the electrostatic interactions characterizing the low-energy structures (see discussion below), thus representing a stiff disordered polymer segment. Note that our statistics show that high total helicity (>50%) persists as high as  $T \approx 500$  K, while the experiments observe high helicity only near T = 273 K [8, 9]. This shift in helix-coil transition temperature is presumably due to the fact that our energy functions including the solvent model are not accurate enough to reproduce the absolute temperature dependence of experiments. As discussed below in detail, our simulation results around T = 400 K best reproduce the NMR experiments (which were conducted at T = 276 K).

In Fig. 3 the end-to-end distance distribution is shown at the same four temperatures as in Fig. 1. Here, the end-to-end distance is defined to be the distance between N of Ala-1 and O of Ala-13. At the two lower temperatures ( $T=276~{\rm K}$  and 370 K) we observe three peaks in the distributions, which suggests that there exist three groups of similar conformations. We refer to the three groups as Groups 1, 2, and 3 from left to right in the Figure. Representative conformations from each group (the lowest-energy conformation in each group) are also shown in Fig. 3. All these three groups of conformations have a common  $\alpha$ -helix structure in residues 5-11. The end-to-end distance is about 1.5 nm, 2 nm, and 2.5 nm for Group 1, Group 2, and Group 3, respectively. Conformations in Group 1 are characterized by a salt bridge between side chains of Glu 2<sup>-</sup> and Lys 7<sup>+</sup> and a bend towards the N-terminus so that the end-to-end distance is the shortest among the three groups. Conformations in Group 2 are characterized by two salt bridges between

Glu  $2^-$  and Lys  $7^+$  and between Glu  $2^-$  and Arg  $10^+$ . Note that this group has the most similarity to the X-ray structure [30], which also has the Glu 2-Arg 10 salt bridge. The backbone root-mean-square distance of the Group 2 structure in Fig. 3 from that of X-ray experiments is 0.12 nm, while those of Group 1 and Group 3 are 0.32 nm and 0.19 nm, respectively. Finally, conformations of Group 3 also have a salt bridge between Glu  $2^-$  and Lys  $7^+$ . However, the N-terminus is pushed away from the  $\alpha$ -helix and the structure is rather extended.

As is shown in Fig. 3, the highest populated peak at the lowest temperature (276 K) corresponds to Group 1. As temperature increases (370 K), this peak decreases in population and the peak of Group 2 increases, thus showing an increased stability of a longer  $\alpha$ -helical segment (characterized by a larger end-to-end distance). At the third temperature (504 K) only a single peak (of Group 2) exists, which suggests that the "native-like" structure (i.e., Group 2) is the most stable among the three groups. At the highest temperature (686 K) we have a single peak at a different end-to-end distance (about 2.2 nm), which corresponds to a coil structure.

The above results can be explained in terms of microscopic interactions. Glu 2 is involved in salt bridges with Lys 7 and, less frequently, with Arg 10. These salt bridges bend the N-terminus toward the short  $\alpha$ -helical region in residues 6-12 and tend to make the whole molecule more compact. These interactions are more efficient at the low temperatures (276 K). Increasing the temperature, the observed salt bridges become less populated and the bending is more frequently released, thus allowing an increase of the molecular extension and, eventually, a more extended  $\alpha$ -helical region including the Ala-Ala-Ala sequence. These extended  $\alpha$ -helical configurations are actually present in the statistics and are characterized by an end-to-end distance of about 2.5 nm. Beyond 500 K, the hydrophobic interactions mainly responsible for the  $\alpha$ -helical stability are no more effective. On the other hand, the salt bridge between Glu 2 and Lys 7 is still contained in the statistics (although it is weaker).

We now study the effects of this conformational distribution and of its temperature dependence on the NOESY CPs. The NOESY experiment was performed at the temperature of 276.15 K, pH 5.2, in the static magnetic field corresponding to  $\nu(^1H) = 500$  MHz, and using a mixing time of 400 ms. These experimental CPs are reported in reference [9]. Unfortunately, the experimental results are reported in arbitrary units and do not allow a quantitative estimate of global dynamical effects, but it is possible to analyze the behaviour of CPs for different proton pairs in the molecule.

The experimental CPs are reported for three types of proton pairs: HN(i)-HN(i+1) (referred to as NN CPs, hereafter),  $H_{\alpha}(i)-HN(i+1)$  (AN CPs, hereafter), and some long-range CPs involving side chains (LR CPs, hereafter). First, the NN CPs were computed at four different temperatures that were used in the REMC simulation (i.e., 276, 370, 504 and 686 K). The above analysis of several statistical quantities, such as the helicity for each residue at each temperature (Fig. 1) showed that the molecular model undergoes a helix-coil structural transition with a transition temperature estimated between 450 K and 600 K (Fig. 2). The real sample undergoes the same transition at lower temperatures; the experimental NOESY CPs are not observable even at room temperature. In Figs. 4(a) and 4(d) the behaviour of the NN and AN CPs with temperature is shown. In both NN and AN data sets, negative CPs are present for the lowest temperature. The experimental NOESY pulse-sequence is phase-sensitive and CPs of opposite sign with respect to the diagonal peaks are not observed at the experimental conditions. Explanation of the change

in sign of the CPs is not trivial. The explanation in terms of a global  $\tau$ , which is the inverse of the unique relaxation rate usually assumed to govern the 2nd-rank rotation of the given H-H distance vector, is here not meaningful, because of the high flexibility that allows many rates to play a significant role in each spectral density. The change in sign of CPs can be related to the change in the whole 2nd-rank rate spectrum that is obtained by the calculations (data not shown); at the lower temperature the spectrum is characterized by several gaps that are progressively smoothed by increasing temperature. It is expected that for the highest temperature the spectrum be almost a smooth function of the relaxation mode as in a polymer random coil. The intermediate situations, where the internal kinetics is faster, but the molecule is still characterized by groups of internal modes separated by rate gaps, can produce the change of sign in CPs and CPs relatively high in magnitude, as in the experiments. On the other hand, the large CPs calculated at high temperatures (e.g., the results at T = 686 K in Fig. 4) can be related to the limitations of the basis set construction in the MCA approximation (i.e., e=5).

Even if the orientational mobility of the H-H unit vector and the H-H average distances are coupled in the TCF of Eq. (7), the behaviour of CPs with temperature can be partially understood in terms of the correlation time (Eq. (9)) and of the average H-H distances. In Figs. 4(b) and 4(e) the correlation times for the NN and AN unit vectors are respectively plotted, and in Figs. 4(c) and 4(f) the average moduli of the same proton pairs are plotted. Correlation times globally decrease as is expected. The decrease in orientational rigidity of the low-temperature helical region occurs up to the highest temperature where the difference in orientational rigidity between residues 1-3 and 4-11 is not significant, as it is expected for a non-structured molecule. On the other hand, it must be noticed that the distances behave differently: The differences between distances in the two regions disappear at the highest temperature, but the distances are still small enough to give contribution to the CPs, especially the AN CPs. Therefore, the structural information contained in CPs must be searched in the behaviour of both sets of CPs, and a separate analysis of AN and NN CPs may be misleading.

The orientational mobility is more sensitive to temperature than the average distances, the latter being more stable. However, it is evident that the approximation of assuming the same orientational behaviour for all the H-H vectors along the sequence does not hold; at 370 K an increase of  $\tau$  from 50 ps to 300 ps moving the H-H vector from the N-terminus deep into the  $\alpha$ -helix (Phe 8) can be observed.

As a consequence of the analysis of the temperature behaviour of CPs, the statistics between 370 K and 504 K can be considered to reproduce the experimental conditions at T=276.15 K. A shift in the order-disorder transition temperature with respect to experiments is expected and always occurs in other simulated systems like liquid crystals.

In Fig. 5 CPs at four selected temperatures are compared with the available experimental data. All calculated and measured CPs are scaled by a unique factor in order to have the AN CP of Ala 3, which is the largest experimental CP available, equal to 1. The increase of NN CPs from the N-terminus to the helical region (residues 6-12) is reproduced by calculations at T = 370 K, with the largest deviations beyond Phe 8 (Fig. 5(a)). The significant decrease of AN CPs beyond residue 3 is qualitatively reproduced (Fig. 5(b)); CPs beyond residue 5 are slightly smaller than those found in the experiments and the largest deviations from experiments is found for Ala 4. This latter deviation is also found in the  $^3J(\text{HN-H}_{\alpha})$  coupling constants (data not shown). The Coupling constants have been computed using the Karplus equation  $^3J = 1.9 - 1.4 \cos(\phi') + 6.4 \cos(\phi')$  where

 $\phi'$  is the HN-N-C<sub> $\alpha$ </sub>-H<sub> $\alpha$ </sub> dihedral angle. Residue Ala 4 presents the largest deviations from experiments, thus implying that the torsional state in the region 4-5 is not well captured by the simulation.

It must be noticed that NN CPs are better reproduced at 370 K, while AN CPs seem to be better reproduced at 432 K. This suggests that a qualitative reproduction of both sets of CPs could be achieved at an intermediate temperature.

The computed LR CPs are all weak; the strongest one ( $H_{\beta}(Thr 3)$ -HN(Ala 5) at  $T=370~\rm K$ ) is  $1.2\times10^{-3}$  compared to the experiment where it is found to be about the same order of magnitude of the NN CPs. These low CPs are caused by the large average distances, because the orientational correlation times of LR H-H unit vectors are in the range 100-200 ps, therefore only slightly smaller than those of NN H-H unit vectors in the helix (about 200 ps, see Fig. 4(e)). On the other hand, the  $H_{\beta}(3)$ -HN(5) average distance is  $0.5\pm0.1~\rm nm$ , which is too large to produce even a weak CP. However, the Glu 2-Lys 7 salt bridge that was suggested by these long range NMR constraints is found very stable up to  $T=432~\rm K$  in the model (0.4 nm), while it becomes 0.5 nm at the highest analyzed temperature. Therefore, even if the NMR structural details are not reproduced in terms of H-H distances, the global features that are responsible for the most populated conformations are contained in the model up to the temperature where the comparison between experimental and computed NN and AN CPs is qualitatively good.

# 4 Conclusions

In this work two recent advances in statistical mechanics have been combined together in the study of the statistics and dynamics of a small peptide, the C-peptide of ribonuclease A. The replica-exchange Monte Carlo simulation has been used to sample molecular configurations in the canonical ensemble at several temperatures in the range 200-800 K. This method, together with other generalized-ensemble algorithms, has the advantage of allowing the overtaking of energy barriers, connecting low temperature and high temperature trajectories. Diffusion theory in the form of the Smoluchowski equation for the conditional probability governing the stochastic time evolution of intramolecular segments' orientation, has then been used to model the orientational correlation functions and to compute the <sup>1</sup>H-NOESY NMR cross peaks that are experimentally available.

The combination of generalized-ensemble statistics and diffusion theory, frequently updated by technical progresses making both methods more robust and efficient, allows the direct calculation of NMR data and other dynamical properties, thus closing the gap between theoretical or computational models and experiments.

#### Acknowledgements:

This work has been done within the bilateral agreement for scientific and technological cooperation between the National Research Council (Italy) and the Japan Society for the Promotion of Science (JSPS). The authors thank Angelo Perico (CNR) for many suggestions on this work. The simulations were performed on the computers at the Research Center for Computational Science, Okazaki National Research Institutes. This work was supported, in part, by a grant from the Research for the Future Program of the Japan Society for the Promotion of Science (JSPS-RFTF98P01101).

# References

- [1] A. Mitsutake, Y. Okamoto, J. Chem. Phys. 112 (2000) 10638.
- [2] Y. Okamoto, M. Masuya, M. Nabeshima, T. Nakazawa, Chem. Phys. Lett. 299 (1999) 17.
- [3] M. Gō, Nature 291 (1981) 90.
- [4] Y. Okamoto, Comp. Phys. Comm. 142 (2001) 55.
- [5] A. Mitsutake, Y. Sugita, Y. Okamoto, Biopolymers (Pept. Sci.) 60 (2001) 96.
- [6] S. Fausti, G. La Penna, J. Paoletti, D. Genest, G. Lancelot, A. Perico, J. Biomol. NMR 27 (2001) 333.
- [7] G. La Penna, P. Carbone, R. Carpentiero, A. Rapallo, A. Perico, J. Chem. Phys. 114 (2001) 1876.
- [8] K.R. Shoemaker, P.S. Kim, D.N. Brems, S. Marqusee, E.J. York, I.M. Chaiken, J.M. Stewart, R.L. Baldwin, Proc. Natl. Acad. Sci. U.S.A. 82 (1985) 2349.
- [9] J.J. Osterhout, Jr., R.L. Baldwin, E.J. York, J.M. Stewart, H.J. Dyson, P.E. Wright, Biochemistry 28 (1989) 7059.
- [10] R. Brüschweiler, D. Morikis, P.E. Wright, J. Biomol. NMR 5 (1995) 353.
- [11] Y. Okamoto, M. Fukugita, T. Nakazawa, H. Kawai, Protein Eng. 4 (1991) 639.
- [12] K.V. Soman, A. Karimi, D.A. Case, Biopolymers 33 (1993) 1567.
- [13] M. Schaefer, C. Bartels, M. Karplus, J. Mol. Biol. 284 (1998) 835.
- [14] U.H.E. Hansmann, Y. Okamoto, J. Phys. Chem. B 103 (1999) 1595.
- [15] G. Lipari, A. Szabo, J. Am. Chem. Soc. 104 (1982) 4546.
- [16] K. Hukushima, K. Nemoto, J. Phys. Soc. Jpn. 65 (1996) 1604.
- [17] Y. Sugita, Y. Okamoto, Chem. Phys. Lett. 314 (1999) 141.
- [18] A. Mitsutake, M. Kinoshita, Y. Okamoto, F. Hirata, submitted for publication.
- [19] Y. Sugita, A. Kitao, Y. Okamoto, J. Chem. Phys. 113 (2000) 6042.
- [20] J. Cavanagh, W.J. Fairbrother, A.G. Palmer III, N.J. Skelton, Protein NMR Spectroscopy, Academic Press, San Diego, 1996.
- [21] M.E. Rose, Elementary Theory of Angular Momentum, John Wiley & Sons, New York, 1957.
- [22] G. La Penna, R. Pratolongo, A. Perico, Macromolecules 32 (1999) 506.
- [23] A. Perico, R. Pratolongo, Macromolecules 30 (1997) 5958.

- [24] M.J. Sippl, G. Némethy, H.A. Scheraga, J. Phys. Chem. 88 (1984) 6231, and references therein.
- [25] Y. Okamoto, Biopolymers 34 (1994) 529.
- [26] T. Ooi, M. Oobatake, G. Némethy, H.A. Scheraga, Proc. Natl. Acad. Sci. USA, 84 (1987) 3086.
- [27] M. Masuya, manuscript in preparation; see also http://biocomputing.cc/.
- [28] R.W. Pastor, M. Karplus, J. Phys. Chem. 92 (1988) 2636.
- [29] K.S. Kostov, K.F. Freed, J. Chem. Phys. 106 (1997) 771.
- [30] R.F. Tilton, Jr., J.C. Dewan, G.A. Petsko, Biochemistry 31 (1992) 2469.
- [31] R. Koradi, M. Billeter, K. Wüthrich J. Mol. Graphics. 14 (1996) 51; the program is available from http://www.mol.biol.ethz.ch/wuthrich/software/molmol/.

### **Figure Captions**

- Figure 1. Average helicity as a function of residue number at four temperatures:  $T=276~\mathrm{K}$  (solid line),  $T=370~\mathrm{K}$  (dashed line),  $T=504~\mathrm{K}$  (dotted line) and  $T=686~\mathrm{K}$  (dotted-dashed line).
- Figure 2. Average total helicity as a function of temperature.
- Figure 3. Distribution of the end-to-end distance at four temperatures: T=276 K (solid line), T=370 K (dashed line), T=504 K (dotted line) and T=686 K (dotted-dashed line); the arrows identify the peaks in terms of representative conformations. Besides backbone, the side chains of Glu 2, Lys 7, and Arg 10 are also shown. The conformations were drawn with MolMol [31].
- Figure 4. NN (a-c) and AN (d-f) CPs, correlation times  $\tau$ , and average H-H distances as functions of residue number: T=276 K (squares), T=370 K (circles), T=504 K (triangles) and T=686 K (diamonds).
- Figure 5. NN (a) and AN (b) CPs as functions of residue number: experimental data (filled squares) and calculated data at  $T=276~{\rm K}$  (squares),  $T=370~{\rm K}$  (circles),  $T=432~{\rm K}$  (triangles), and  $T=504~{\rm K}$  (diamonds).

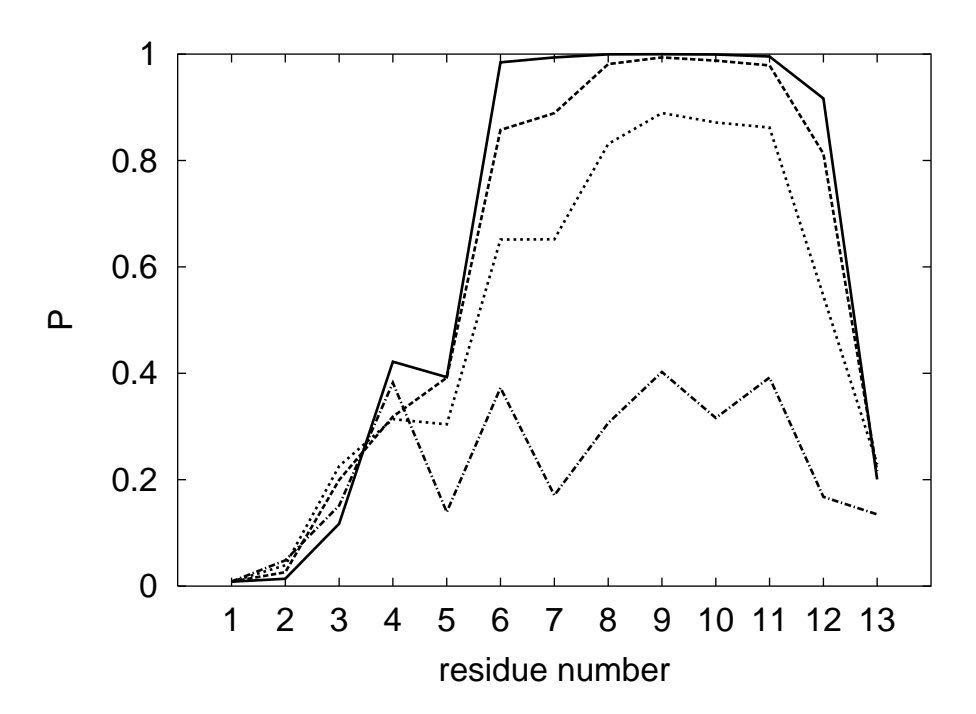


Figure 1: La Penna et al.

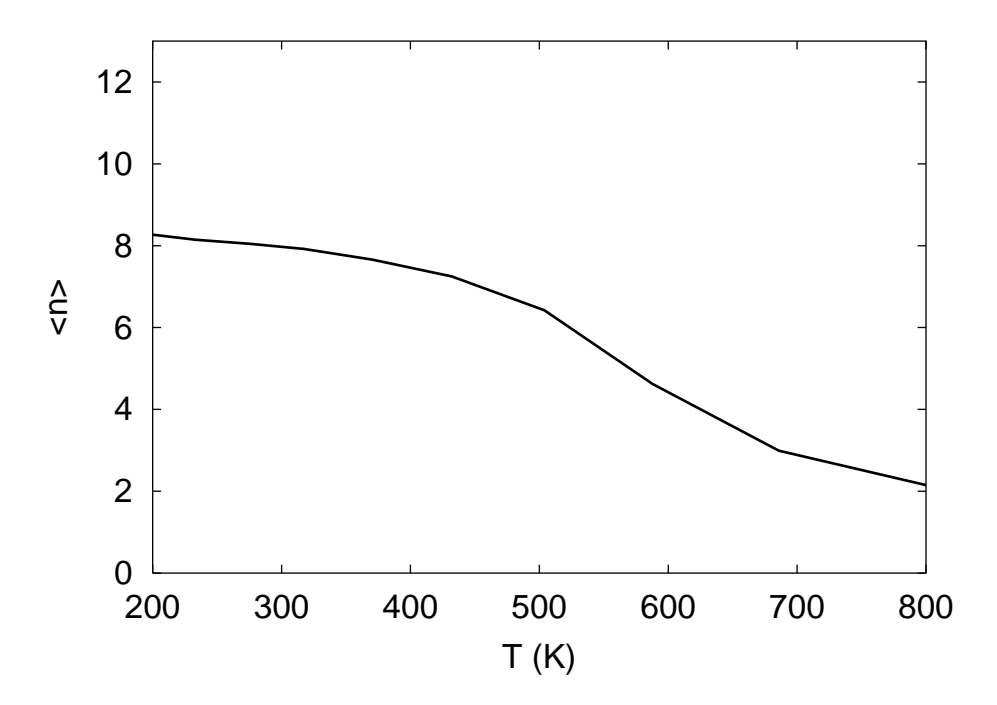


Figure 2: La Penna et al.

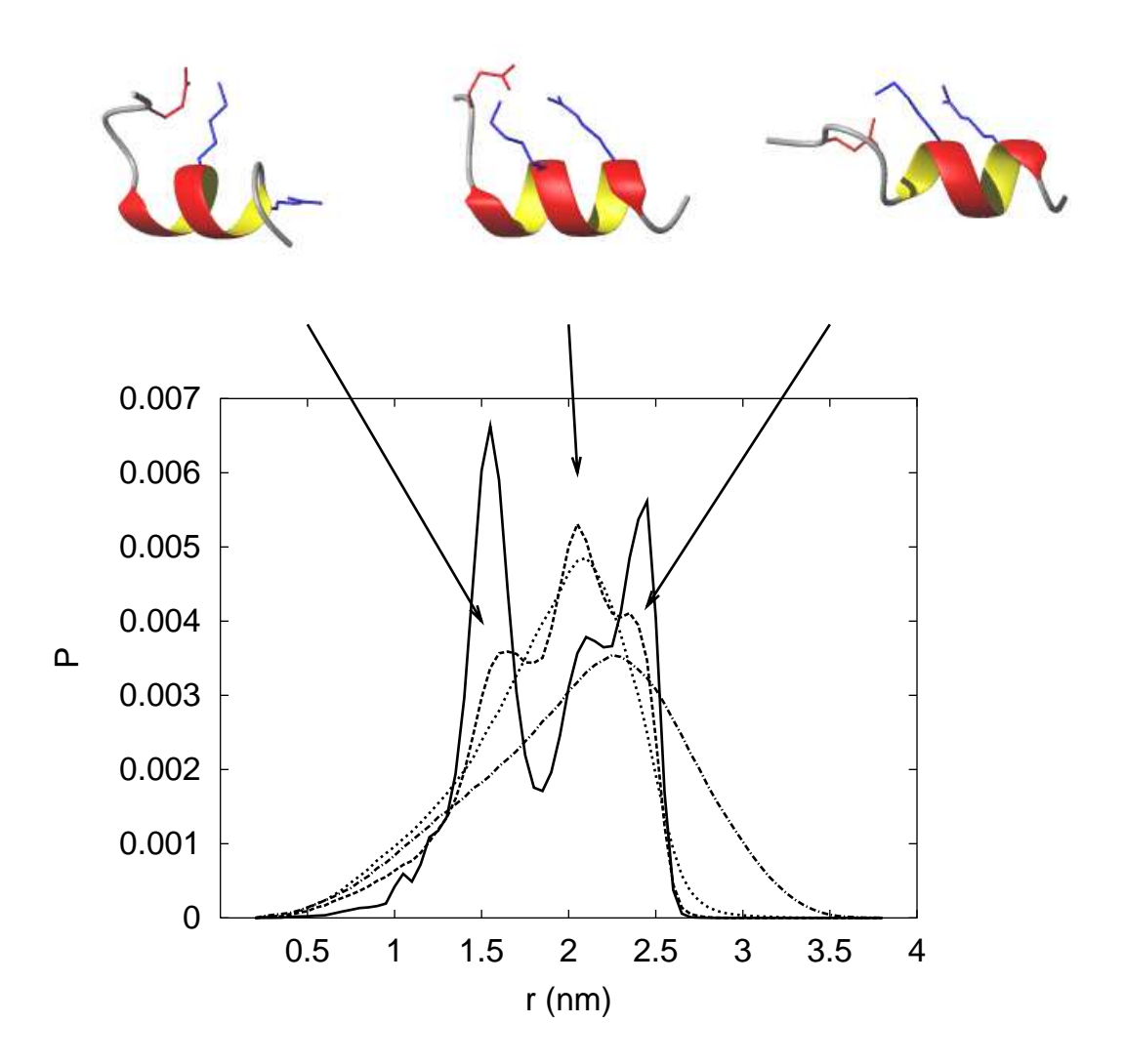


Figure 3: La Penna et al.

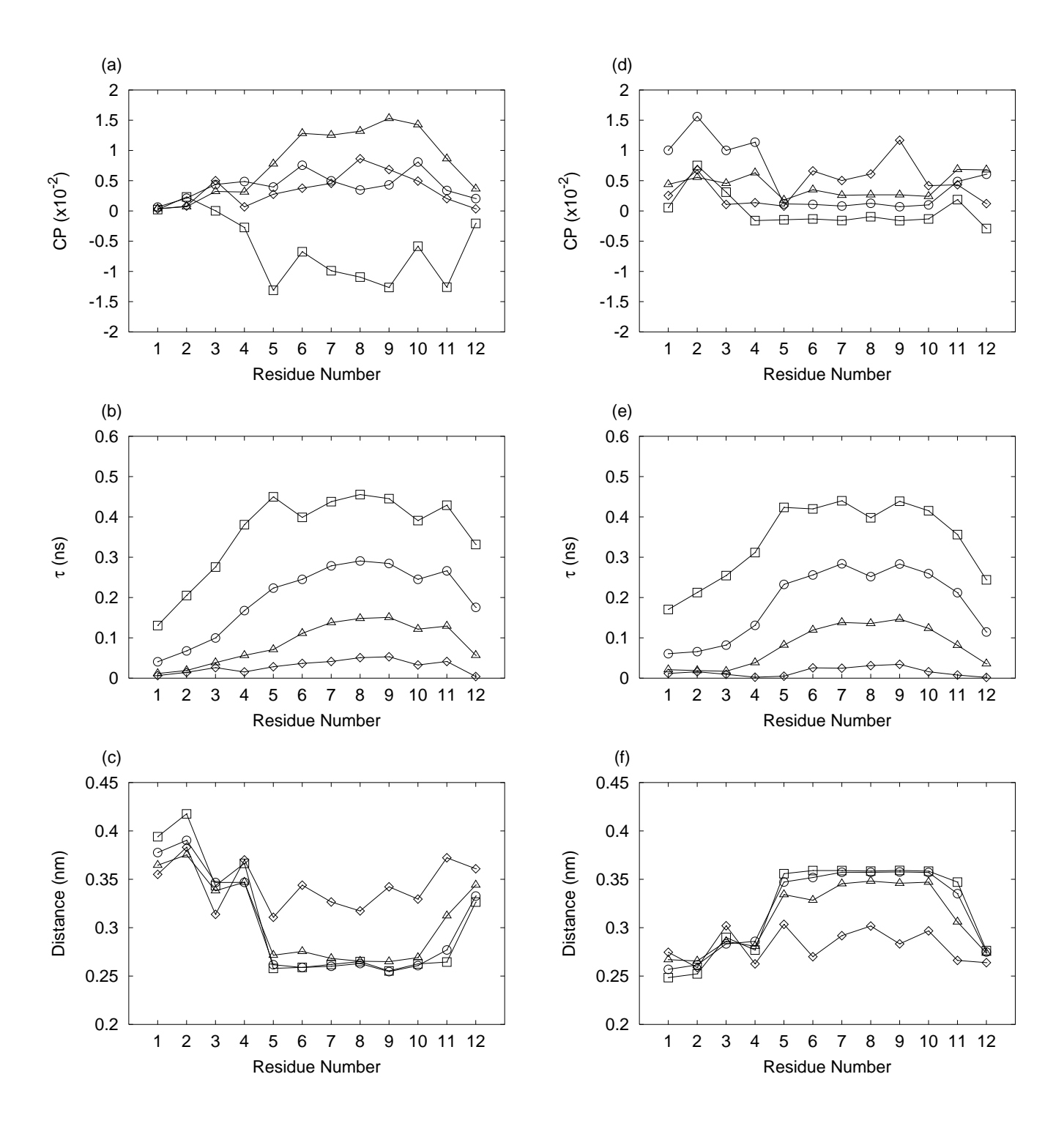


Figure 4: La Penna et al.

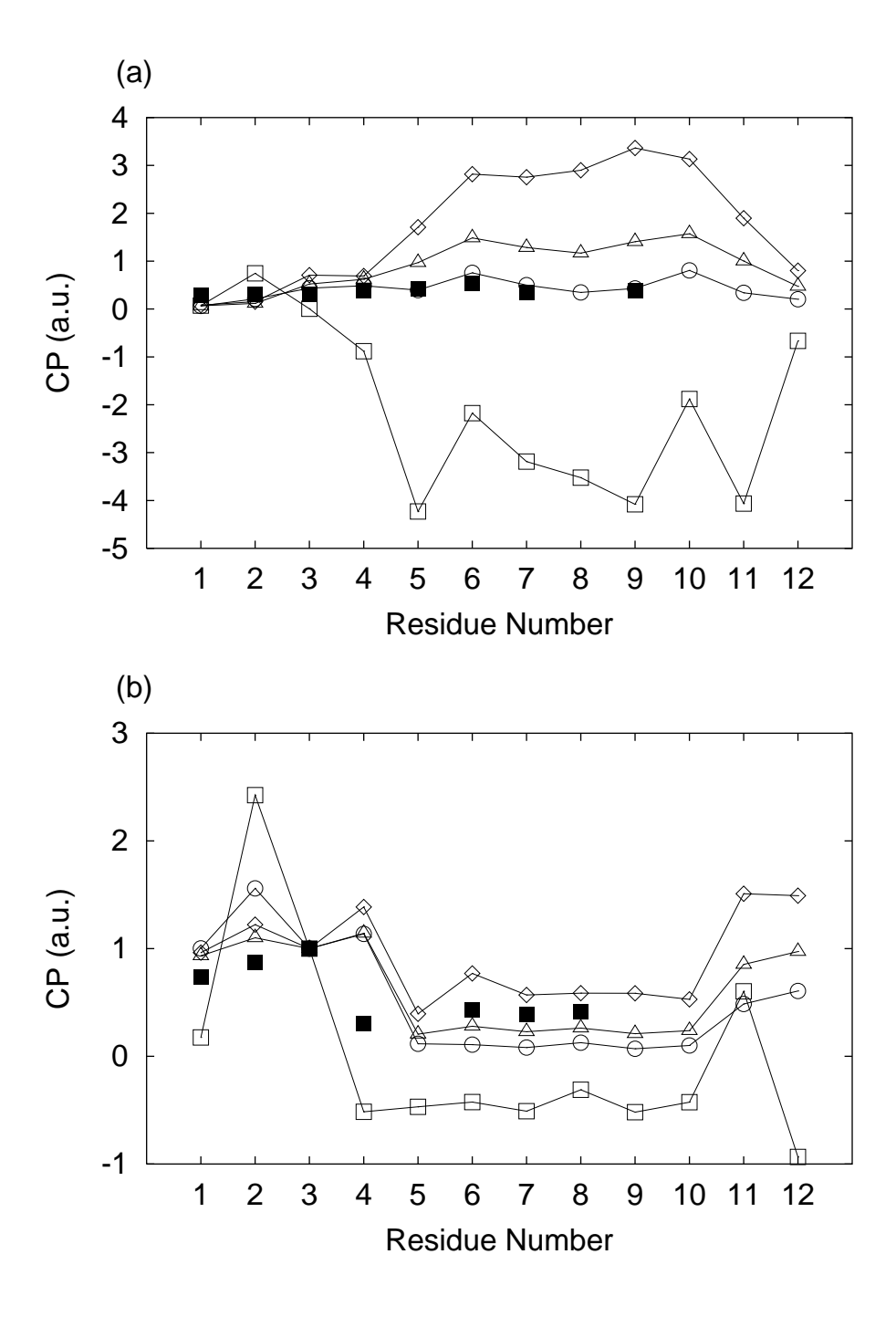


Figure 5: La Penna et al.